**Atmospheric
Chemistry
and Physics
Discussions**

Bounce behavior of freshly nucleated biogenic secondary organic aerosol particles

A. Virtanen[1], J. Kannosto[1], J. Joutsensaari[2], E. Saukko[1], H. Kuuluvainen[1],
L. Hao[2], P. Yli-Pirilä[3], P. Tiitta[2], J. K. Holopainen[3], D. R. Worsnop[2,4,5],
J. N. Smith[2,6,7], and A. Laaksonen[2,4]

[1]Tampere University of Technology, Department of Physics, P.O. Box 692, 33101 Tampere, Finland
[2]University of Eastern Finland, Department of Applied Physics, P.O. Box 1627, 70211 Kuopio, Finland
[3]University of Eastern Finland, Department of Environmental Science, P.O. Box 1627, 70211 Kuopio, Finland
[4]Finnish Meteorological Institute, P.O. Box 503, 00101 Helsinki, Finland
[5]Aerodyne Research, Billerica, MA 08121-3976, USA
[6]Finnish Meteorological Institute, P.O. Box 1627, Kuopio, Finland
[7]National Center for Atmospheric Research, P.O. Box 3000, Boulder, CO 80307, USA

Title Page

Abstract | Introduction

Conclusions | References

Tables | Figures

|◄ | ►|

◄ | ►

Back | Close

Full Screen / Esc

Printer-friendly Version

Interactive Discussion

Correspondence to: A. Virtanen (annele.virtanen@tut.fi)

Bounce behavior of freshly nucleated biogenic SOA particles

A. Virtanen et al.

Full Screen / Esc

Abstract

The assessment of the climatic impacts and adverse health effects of atmospheric aerosol particles requires detailed information on particle properties. However, very limited information is available on the morphology and phase state of secondary organic aerosol (SOA) particles. The physical state of particles greatly affects particulate-phase chemical reactions, and thus the growth rates of newly formed atmospheric aerosol particles. Thus verifying the physical phase state of SOA particles gives new and important insight into their formation, subsequent growth, and consequently potential atmospheric impacts. According to our recent study, biogenic SOA particles produced in laboratory chambers from the oxidation of real plant emissions as well as in ambient boreal forest atmospheres can exist in a solid phase in size range >30 nm. In this paper, we extend previously published results to diameters in the range of 17–30 nm. The physical phase of the particles is studied by investigating particle bounce properties utilizing electrical low pressure impactor (ELPI). We also investigate the effect of estimates of particle density on the interpretation of our bounce observations. According to the results presented in this paper, particle bounce clearly decreases with decreasing particle size in sub 30 nm size range. The decreasing bounce can be caused by the differences in composition and phase of large (diameters greater than 30 nm) and smaller (diameters between 17 and 30 nm) particles.

1 Introduction

Secondary aerosol formation via nucleation of precursor vapors and subsequent condensational growth has been reported to produce atmospheric aerosol particles in a variety of environments (e.g., Kulmala et al., 2004; Laaksonen et al., 2005). Numerous modelling studies (e.g., Spracklen et al., 2006) suggest that these particles are likely to have a significant impact on climate. The assessment of the climatic impacts and adverse health effects of atmospheric aerosol particles require detailed information on

particle properties. Oxidation products of volatile organic compounds (VOC) emitted by sources such as vegetation participate in the formation and growth process of the newly formed atmospheric particles (Laaksonen et al., 2008; Kanakidou et al., 2005; Jimenez et al., 2009; Claeys et al., 2004). These are called secondary organic aerosol (SOA). Recent estimates on the importance of SOA formation show that it may be as significant as primary organic aerosol emissions, comprising about 60–70% of the organic aerosol mass on the global scale and regionally even higher (Hallquist et al., 2009; Kanakidou et al., 2005). Furthermore, substantial formation of biogenic SOA takes place over the boreal forest in northern Europe, indicating that the forest is a major source of climate-relevant aerosol particles (Tunved et al., 2006). SOA formation and properties are widely studied to clarify the role of SOA in radiative forcing and climate. In spite of their importance, the exact species and mechanisms that are responsible for the formation and growth of SOA is still not known. This is especially true for sub-30 nm diameter particles, for which the Kelvin effect predicts that a relatively small subset of available aerosol precursors participate in gas-particle partitioning due to their volatility.

It is well known that inorganic salts such as $NH_4(SO_4)_2$ and NaCl can be found in liquid droplets or solid crystals in the atmosphere depending on the surrounding humidity and temperature (e.g., Martin, 2000). However, very limited information is available on the morphology and phase state of SOA particles. According to our recent study, biogenic SOA particles produced in laboratory chamber from the oxidation of real plant emissions as well as in ambient boreal forest atmospheres can exist in a solid phase (Virtanen et al., 2010). In addition, the results of Cappa and Wilson (2010) indicate that the SOA particles formed through α-pinene ozonolysis might be in a solid amorphous state rather than liquid. The physical state of particles greatly affects chemical reactions in the particles, and thus the growth rates of newly formed atmospheric aerosol. For highly viscous and solid particles, chemical reactions are typically surface-limited (i.e., heterogeneous reaction on particle surfaces). Zobrist et al. (2008) and others (Murray, 2008; Mikhailkov et al., 2009) also suggested that the water uptake of the

Bounce behavior of freshly nucleated biogenic SOA particles

A. Virtanen et al.

Title Page

Abstract	Introduction
Conclusions	References
Tables	Figures

|◀ | ▶|

◀ | ▶

Back | Close

Full Screen / Esc

Printer-friendly Version

Interactive Discussion

particles is diminished or even fully inhibited for highly viscous or glassy aerosols. In gas-to-particle partitioning models developed for SOA particles, it is generally assumed that particles are in liquid state (Pankow, 1994; Odum et al., 1996). Thus verifying the physical phase state of SOA particles gives new and important insight into their forma-
5 tion and growth process and essential information on their atmospheric impacts.

The physical phase of the particles can be studied by investigating particle bounce properties (Virtanen et al., 2010). When an aerosol particle collides with an impaction surface, one part of its kinetic energy is dissipated in the deformation process, and another part is converted elastically into kinetic energy of rebound. If the rebound en-
10 ergy exceeds the adhesion energy, the particle will bounce from the surface. Thus both the elastic properties and surface properties of particles affect their bounce probability (Rogers and Reed, 1984). Relative humidity (RH) also affects the bounce probabil-ity as RH influences the viscoelastic properties of hygroscopic aerosol particles (Stein et al., 1994). Generally, harder materials, larger particles or greater impact velocity
15 will lead to a higher bounce probability, although the roughness of the collecting sur-face also plays a significant role (Dahneke, 1971; Chang et al., 1991). In our recent paper (Virtanen et al., 2010) we showed that biogenic SOA particles bounce in im-pactor stages, indicating that the particles are solid in their physical phase. Based on electron diffraction analysis and bounce measurements of liquid, crystalline and amor-
20 phous solid laboratory-generated aerosol, we concluded that biogenic SOA particles larger than 30 nm in diameter are amorphous solids. In this paper, we extend these results to diameters in the range of 17–30 nm. Furthermore, we investigate the effect of estimates of particle density on the interpretation of our bounce observations.

⏮ | ⏭

◀ | ▶

Back | Close

Full Screen / Esc

Printer-friendly Version

Interactive Discussion

2   Methods

2.1   Chamber experiments

The SOA experiments were performed at the Kuopio aerosol research chamber using living Scots Pine trees as a natural source of VOCs. The experimental setup has been described in detail by Hao et al. (2009). Briefly, the system consists of a plant enclosure (fluorinated ethylene propylene (FEP) bag), a reaction chamber (made also of FEP film with a volume of $6\,m^3$), and gas and particle measurement systems that are described in greater detail below. All branches with green needles on a 10-year-old Scots Pine seedling were enclosed in an FEP bag, which was sealed on the stem bark. Plant-emitted VOCs were transported by purified and dried air into the separate reaction chamber in order to achieve the desired concentration of VOCs. To simulate herbivore attack on tree bark and to activate the chemical defence of seedlings, thereby enhancing VOC emissions, 1 cm long and 1 mm deep cuts were made on the base of the main stem by a knife.

Table 1 summarizes the experiments conducted in this research. Two experiments were performed in the current study. In experiment (1) ozone-initiated chemistry was explored, whereas in experiment (2) tetramethylethylene (TME) was added to the chamber to produce additional hydroxyl radicals (OH) and increase the $OH:O_3$ ratio (i.e., oxidation conditions) in the reaction chamber (Lambe et al., 2007). In experiment (2) 1 ppm of SO_2 in nitrogen was also added to the chamber. After injecting the plant-derived VOCs, 700 ppb of ozone generated by a UV lamp O_3 generator was added to the chamber at a flow of 40 Lpm for approximately 8 min. In all experiments, the temperature (T) was $22\pm1\,°C$ and relative humidity (RH) was controlled in the range of $30\pm5\%$ (measured with Vaisala Humidity and Temperature Probe HMP50). Ozone (DASIBI 1008-RS O_3 analyzers, Dasibi Environmental Corporation), NO_x (AC 30 M NO_x analyzer Environment s.a.), SO_2 (AF21M SO_2 analyzer Environment s.a.) and VOC concentrations were measured inside the chamber during experiments. VOC samples were collected on Tenax-TA adsorbent and the samples were analyzed by

gas chromatography-mass spectrometry (Vuorinen et al., 2004). The initial VOC concentrations inside the chamber before ozone addition were 18.8 ppb and 107.6 ppb for the ozone O_3 (exp. #1) and OH + SO_2 (exp. #2) experiments, respectively. To increase aerosol mass loading in the experiment (1), two extra ozone injections were made at two hours after the first ozone addition.

The particle size distributions were measured by two scanning mobility particle sizers (SMPS) comprised of a Differential Mobility Analyzer (DMA; model 3081, TSI, Inc.) coupled to a condensation particle counter (CPC; model 3022, TSI, Inc.) and a nano DMA (model 3085, TSI, Inc.) coupled to a ultrafine CPC (model 3027, TSI, Inc.) with mobility diameter ranges of 10–700 nm and 3–60 nm, respectively. Furthermore, chemical composition and mass size distributions of aerosol particles formed during the experiments were measured with a quadrupole-based Aerosol Mass Spectrometer (AMS, Aerodyne Inc.). The average density of particles was determined by comparing the SMPS volume and AMS mass size distributions (De Carlo et al., 2004).

The size distributions and bounce behaviour of particles, which is related to particle physical phase state, were determined with an electrical low pressure impactor (ELPI). In ELPI, particles are charged by a unipolar corona charger and after the charger, the particles enter a twelve stage cascade impactor (Keskinen et al., 1992), where the particles are classified according to their aerodynamic size, depending on both the physical size and the density of the particle. In a conventional ELPI set-up, the cut size of the lowest stage is approximately 30 nm, however for these investigations the ELPI was equipped with an additional impactor stage with a cut-off size of 17 nm. In addition, a back-up filter was used to measure particles smaller than the lowest impactor cut-off size.

2.2 Particle bounce analysis

In the normal operation of a cascade impactor, particle bounce perturbs the measurement as larger particles are transferred to lower stages following bounce thus biasing the inferred size distribution towards smaller sizes. When particle bounce occurs in an

ELPI, a significant excess current is measured in the lowest impactor stages resulting from the charges carried by the bounced particles. An example of a bounce-perturbed distribution is shown in Fig. 1b (black lines), where the measured ELPI currents are shown for SOA formed from OH oxidation products of pine emissions in the presence of SO_2 (Virtanen et al., 2010). The average particle size was 100 nm and the geometric standard deviation of the unimodal distribution was 1.27 during the measurement, i.e. there were no small particles (≤ 30 nm) present in the aerosol, see Fig. 1a. Nevertheless, a significant excess current was measured in the lowest impactor stages when the smooth impactor substrates were used (black histogram in Fig. 1b). When the smooth substrates were replaced by porous substrates thus reducing the bounce (Chang et al., 1991), no excess current was measured in the lowest stages (red bars in Fig. 1b).

As shown in Fig. 1b, particle bounce perturbs the measurement as a result of the transfer of particles to lower impactor stages. Hence, particle bounce can be quantified by analyzing the difference in bounce-affected measured currents with ideal non-affected currents. To calculate the ideal currents the measured SMPS number distribution as a function of particle diameter, $n_{SMPS}(d_p)$, is converted to ELPI current response $i^{id}(d_p)$ by first multiplying the measured SMPS distribution by the ELPI charger efficiency curve, $E_{ch}(d_p)$ (Ristimäki et al., 2002)

$$i^{id}(d_p) = n_{SMPS}(d_p)E_{ch}(d_p) \tag{1}$$

Next, the resulting current distribution i^{id} is passed through the ELPI impactor kernel functions k_j to mimic the particle collection within the impactor (Ristimäki et al., 2002). The kernel functions are carefully calibrated for chosen impactor units and substrate types. The current in the jth impactor stage can be calculated from the following equation:

$$I_j^{id} = \int_0^\infty k_j(d_p, \rho)i^{id}(d_p)d\,d_p \tag{2}$$

Such calculations result in idealized ELPI currents. In the above calculations, the average particle density (ρ) is required. For pine derived SOA particles measured in the smog chamber we use densities obtained from AMS-SMPS measurements (density value of $1.1 \, \mathrm{g \, cm^{-3}}$). Note that the particle density was determined for particle diameters larger than 100 nm due to low mass loadings in the chamber and the low particle transmission efficiency of the AMS for particles smaller than 40 nm.

When the measured and ideal currents are compared, the fraction of excess current in the back-up filter can be estimated. This fraction is called the bounce factor (Virtanen et al., 2010). In the measurements reported by Virtanen et al. (2010), the bounce factor was determined reliably only for particles having GMD larger than 30 nm. This was due to the fact that the lowest cut size of the impactor set-up used in atmospheric measurements was 30 nm. If the ELPI is equipped with additional impactor stage having cut-size 17 nm (Yli-Ojanperä et al., 2010), it is possible to extend the bounce characteristic investigations down to 17 nm according to (see also Fig. 2)

$$\text{bounce factor} \equiv \frac{I_{\text{filter}} - I_{\text{filter}}^{\text{id}}}{\sum I_{\text{impactor stages} \geq 17 \, \text{nm}}^{\text{id}}}, \tag{3}$$

where I_{filter} is the current measured in back-up filter, $I_{\text{filter}}^{\text{id}}$ is the simulated ideal current in back up filter, and $\sum I_{\text{impactor stages} \geq 17 \, \text{nm}}^{\text{id}}$ is the sum of the ideal currents calculated from the impactor stages (excluding the back-up filter). Here the cut size of the last impactor stage is 17 nm.

3 Results and discussion

For comparison, the normalized bounce factors for 17 and 30 nm size limits are shown in Fig. 2 for particles produced by the OH dominated oxidation of pine emitted VOCs (in presence of added SO_2 in the chamber). The results shown in Fig. 2 are calculated using particle density of $1.1 \, \mathrm{g \, cm^{-3}}$ derived from the AMS-SMPS measurements and

Bounce behavior of freshly nucleated biogenic SOA particles

A. Virtanen et al.

they are shown as a function geometric mean mobility diameter (GMD) of SMPS size distributions. It should be noted, that the absolute value of bounce factors for size limits 17 nm and 30 nm differs because in the 30 nm case, the bounce factor is calculated according to the equation presented in Virtanen et al. (2010) instead of Eq. (3). The size limits of 17 nm and 30 nm are marked with grey vertical lines in the figure. As can be seen, the particle bounce factor clearly decreases in size range below 30 nm.

The particle bounce data can be used to constrain the density of sub-30 nm diameter particles, for which little experimental data is available (Kannosto et al., 2008). In Fig. 3 we show the calculated bounce factor for data obtained with the 17 nm diameter size limit using density values varying from $0.8\,\mathrm{g\,cm^{-3}}$ to $2\,\mathrm{g\,cm^{-3}}$. The results indicate that in spite of possible uncertainties in the density, the bounce of the sub 30 nm particles clearly decreases with decreasing particle size. In addition, the bounce factor for particles $> 40\,\mathrm{nm}$ is insensitive to the chosen density.

In the upper right corner of Fig. 3a,b, the results of the details in bounce factor values for the smallest particle sizes are shown. The zero value for bounce factor is marked with dashed line in the figure. As can be seen, the bounce factor gets clearly negative values when low density values are used in calculations. Underestimating the density in the calculations results in unrealistically high simulated current values in the back up filter compared to the measured currents (i.e., unrealistic high values of $I^{\mathrm{id}}_{\mathrm{filter}}$ in Eq. 3), thus the numerator in Eq. (3) gets negative values. The closer the investigated size is to the cut size of lowest impactor stage (in this case 17 nm) the more sensitive the calculated bounce factor is for the chosen density values.

In the case of particles formed by ozonolysis of pine derived VOC in the absence of SO$_2$ (henceforth referred to as the "O$_3$ case"), the bounce factor achieved positive values for the smallest measured mobility diameter (18 nm) when the density used in calculations are greater than $1.3\,\mathrm{g\,cm^{-3}}$ (Fig. 3a). In the case of OH initiated oxidation in the presence of SO$_2$ (referred to as the "OH + SO$_2$ case"), the corresponding density value is $1.6\,\mathrm{g\,cm^{-3}}$ (Fig. 3b). This indicates that in the experiments with SO$_2$ (OH + SO$_2$ case), the density of the smallest particles is higher than in the absence of SO$_2$ (O$_3$

case). In Fig. 4a the ratio of SO_4^{2-} to organics measured by the AMS is shown for $OH + SO_2$ case. It can be seen that smaller particles contained higher amount of SO_4^{2-} than larger particles. On the other hand, particles formed through ozonolysis in absence of SO_2 contained no SO_4^{2-}. Densities of inorganic compounds containing SO_4^{2-}

5   are typically higher compared to organic compounds, e.g., $1.84\,g\,cm^{-3}$ for sulphuric acid and ca. $1.77\,g\,cm^{-3}$ for ammonium sulphate (Lide, 1996). This can explain the differences in densities of the smallest particles in these two cases. When the density values analyzed for larger particles (50–100 nm) from AMS and SMPS distributions shown in Table 1, no clear differences are observed. As Fig. 4a shows, at these larger

10   sizes the ratio of SO_4^{2-} to organic decreases and particles become more similar to pure SOA.

    The higher density values needed to gain the positive bounce factor (calculated from Eq. 3) for the $OH + SO_2$ case could be explained also by the lower bounced fraction of these particles (i.e., the lower measured current value in the filter stage (I_{filter}) in Eq. 3)

15   when compared to O_3 case. In fact, when the bounce factors in Fig. 3a,b are compared it can be seen that the overall bounce factor for $OH + SO_2$ case is lower than for the O_3. According to our earlier work (Virtanen et al., 2010) the bounce factor measured for ammonium sulphate particles is clearly lower than for amorphous polystyrene or SOA particles. This could be due to the difference in elastic properties of crystalline

20   and amorphous materials or in charge transfer characteristics of these materials. One conclusion that one may draw from our observations that the differences in bounce behaviour of the smallest (around 20 nm) particles in these two investigated cases are related to the SO_4^{2-} concentration in particles. The higher SO_4^{2-} fraction in smallest particles can result in higher density value of the particles or the lower bounce probability

25   of the particles (or both of these). The effect of these differences can be seen in calculated bounce factors. The decrease of the SO_4^{2-} fraction in particles in $OH + SO_2$ case (Fig. 4a) with increasing particle size indicates also that the sulphate compounds play a key role in initial particle formation and the organics participate strongly on particle growth.

Title Page

Abstract | Introduction

Conclusions | References

Tables | Figures

⏮ | ⏭

◀ | ▶

Back | Close

Full Screen / Esc

Printer-friendly Version

Interactive Discussion

According to the results presented here, particle bounce clearly decreases with decreasing particle size. The decreasing bounce can be caused by two reasons. Firstly it is important to note that with decreasing particle size the velocity needed for bounce to occur increases, since the required velocity is inversely proportional to particle size (Dahneke et al., 1971). On the other hand, 17–30 nm particles impact on the lowest impactor stage where the impaction velocities are generally higher than impaction velocities in the upper stage where, e.g., the 40 nm particle impacts for the first time. In addition, the contact velocities of particles impacting onto specific impactor stage depend on particle size: particles clearly larger than the cut point of the impaction stage have higher velocities than particles having size close to the cut point. Note that with two particle populations having exactly the same bounce properties (as a function of particle size) but different size distributions in such a way that the ratios $N(17\,\text{nm})/N(30\,\text{nm})$ (where the N's denote particle concentrations) differ, the bounce from the 17–30 nm might appear different. Specifically, the population with higher $N(17\,\text{nm})/N(30\,\text{nm})$ would probably show less bounce. However, we do not see any obvious effect stemming from size distribution differences in the present experiments. Thus it is not straightforward to predict how the decreasing size affects bounce. A sophisticated impactor flow field model is needed to calculate the impaction velocity distributions for the each particle size as well as to estimate the dependence of bounce on material characteristics of the aerosol. This kind of model is currently under construction and these calculations are planned in the future.

Secondly, the decreasing bounce can be caused by the differences in composition and phase of larger (GMD > 30 nm) and smaller (GMD 17–30 nm) particles. In Fig. 4a,b the ratio of mass of m44 to mass of total organics analyzed from AMS data is shown as a function of GMD of number distribution for the $OH + SO_2$ and O_3 experiments, respectively. It should be noted, that the AMS composition data shown in Fig. 4 is presented as a function of GMD of number distribution measured by SMPS. In the O_3 case, no SO_4^{2-} was detected in AMS signal, as can be expected, but the particle oxidation degree of the smallest particles, as represented by the fraction of the *m/z*

A. Virtanen et al.

Title Page

Abstract | Introduction

Conclusions | References

Tables | Figures

◄◄ | ►►

◄ | ►

Back | Close

Full Screen / Esc

Printer-friendly Version

Interactive Discussion

44 fragment of the total organic mass concentration, is clearly lower than of the larger particles (Fig. 4a). Hence we can assume that the fresher and smaller particles are less oxidized than the larger particles. As a matter of fact, the lower oxidation degree of the smallest particles might be related to the "less solid" nature of the particles: it is known that the oligomers or other organic compounds with high molar mass are more prone to glass formation than smaller molecules (Zobrist et al., 2008). Hydrogen bonding between oxygenated compounds and functional groups may also favour the formation of solid phases (Mikhailov et al., 2009). The potential influence of oxidation on the phase state of organic aerosol particles should be explored in future studies.

In the $OH + SO_2$ case, the measured fraction of particulate SO_4^{2-} increases with decreasing particles size but no clear changes in particle oxidation degree can be observed. As mentioned above, the bounce factor for $OH + SO_2$ case particles containing fraction of SO_4^{2-} is generally lower than bounce factor for O_3 case (no SO_4^{2-} in particles). According to our earlier laboratory experiments (Virtanen et al., 2010) the bounce factor measured for ammonium sulphate particles is clearly lower than for amorphous polystyrene or SOA particles. This could be due to the difference in elastic properties of crystalline and amorphous materials or in charge transfer characteristics of these materials. Hence the increasing fraction of SO_4^{2-} in smallest particles might also result in lowering bounce factor.

4 Conclusions

The results reported here give information on the bounce characteristics (i.e., physical phase state) of smallest SOA particles produced by O_3 initiated oxidation and by OH dominated oxidation with SO_2 added in the chamber. Results suggest that the decrease of bounce might be caused by the differences in particle chemistry and their phase: the smaller (diameters between 17 and 30 nm) particles having lower oxidation degree or containing higher amount of SO_4^{2-} bounced less than larger (diameters greater than 30 nm) particles indicating different material characteristics in the case of

fresher sub 30 nm size particles. The result might indicate that the initial nucleation process and growth of the newly formed particle is driven by mass transfer of molecules from gas phase to liquid phase. When particles are more aged, the solidification takes place and the partitioning process changes. Nonetheless, we can not categorically exclude the possibility that the small particle size by itself causes the decrease of particle bounce probability. To investigate this phenomenon in more detail, the sophisticated impactor flow field model and also estimation on particle characteristics affecting its bounce properties should be at hand. This is the subject of future studies.

References

Cappa, C. D. and Wilson, K. R.: Evolution of organic aerosol mass spectra upon heating: implications for OA phase and partitioning behavior, Atmos. Chem. Phys., 11, 1895–1911, doi:10.5194/acp-11-1895-2011, 2011.

Chang, M., Kim, S., and Sioutas, C.: Experimental studies on particle impaction and bounce effects of substrate design and materials, Atmos. Environ., 33, 2313–2322, 1999.

Claeys, M., Graham, B., Vas, G., Wang, W., Vermeylen, R., Pashynska, V., Cafmeyer, J., Guyon, P., Andreae, M. O., Artaxo, P., and Maenhaut, W.: Formation of secondary organic aerosols through photooxidation of isoprene, Science, 303(5661), 1173–1176, 2004.

Dahneke, B.: Capture of aerosol particles by surfaces, J. Coll. Interface Sci. 37, 342–347, 1971.

De Carlo, P. F., Slowik, J. G., Worsnop, D. R., Davidovits, P., and Jimenez, J. L.: Particle morphology and density characterization by combined mobility and aerodynamic diameter measurements. Part 1: theory, Aerosol Sci. Technol., 38, 1185–1205, 2004.

Hallquist, M., Wenger, J. C., Baltensperger, U., Rudich, Y., Simpson, D., Claeys, M., Dommen, J., Donahue, N. M., George, C., Goldstein, A. H., Hamilton, J. F., Herrmann, H., Hoffmann, T., Iinuma, Y., Jang, M., Jenkin, M. E., Jimenez, J. L., Kiendler-Scharr, A., Maenhaut, W., McFiggans, G., Mentel, Th. F., Monod, A., Prévôt, A. S. H., Seinfeld, J. H., Surratt, J. D., Szmigielski, R., and Wildt, J.: The formation, properties and impact of secondary organic aerosol: current and emerging issues, Atmos. Chem. Phys., 9, 5155–5236, doi:10.5194/acp-9-5155-2009, 2009.

Hao, L. Q., Yli-Pirilä, P., Tiitta, P., Romakkaniemi, S., Vaattovaara, P., Kajos, M. K., Rinne, J., Heijari, J., Kortelainen, A., Miettinen, P., Kroll, J. H., Holopainen, J. K., Smith, J. N., Joutsensaari, J., Kulmala, M., Worsnop, D. R., and Laaksonen, A.: New particle formation from the oxidation of direct emissions of pine seedlings, Atmos. Chem. Phys., 9, 8121–8137, doi:10.5194/acp-9-8121-2009, 2009.

Jimenez, J. L., Canagaratna, M. R., Donahue, N. M., Prevot A. S. H., Zhang, Q., Kroll, J. H., DeCarlo, P. F., Allan, J. D., Coe, H., Ng, N. L., Aiken, A. C., Docherty, K. S., Ulbrich, I. M., Grieshop, A. P., Robinson, A. L., Duplissy, J., Smith, J. D., Wilson, K. R., Lanz, V. A., Hueglin, C., Sun, Y. L., Tian, J., Laaksonen, A., Raatikainen, T., Rautiainen, J., Vaattovaara, P., Ehn, M., Kulmala, M., Tomlinson, J. M., Collins, D. R., Cubison, M. J., Dunlea, E. J., Huffman, J. A., Onasch, T. B., Alfarra, M. R., Williams, P. I., Bower, K., Kondo, Y., Schneider, J., Drewnick, F., Borrmann, S., Weimer, S., Demerjian, K., Salcedo, D., Cottrell, L., Griffin, R., Takami, A., Miyoshi, T., Hatakeyama, S., Shimono, A., Y Sun, J., Zhang, Y. M., Dzepina, K., Kimmel, J. R., Sueper, D., Jayne, J. T., Herndon, S. C., Trimborn, A. M., Williams, L. R., Wood, E. C., Middlebrook, A. M., Kolb, C. E., Baltensperger, U., and Worsnop, D. R.: Evolution of organic aerosols in the atmosphere, Science 326, 1525–1529, 2009.

Kanakidou, M., Seinfeld, J. H., Pandis, S. N., Barnes, I., Dentener, F. J., Facchini, M. C., Van Dingenen, R., Ervens, B., Nenes, A., Nielsen, C. J., Swietlicki, E., Putaud, J. P., Balkanski, Y., Fuzzi, S., Horth, J., Moortgat, G. K., Winterhalter, R., Myhre, C. E. L., Tsigaridis, K., Vignati, E., Stephanou, E. G., and Wilson, J.: Organic aerosol and global climate modelling: a review, Atmos. Chem. Phys., 5, 1053–1123, doi:10.5194/acp-5-1053-2005, 2005.

Kannosto, J., Virtanen, A., Lemmetty, M., Mäkelä, J. M., Keskinen, J., Junninen, H., Hussein, T., Aalto, P., and Kulmala, M.: Mode resolved density of atmospheric aerosol particles, Atmos. Chem. Phys., 8, 5327–5337, doi:10.5194/acp-8-5327-2008, 2008.

Kulmala, M., Vehkamäki, H., Petäjä, T., Dal Maso, M., Lauri, A., Kerminen, V.-M., Bilmili, W., and

McMurry, P.: Formation and growth rates of ultrafine atmospheric aerosol particles: a review of observations, J. Aerosol Sci., 35, 143–176, 2004.

Laaksonen, A., Hamed, A., Joutsensaari, J., Hiltunen, L., Cavalli, F., Junkermann, W., Asmi, A., Fuzzi, S., and Facchini, M. C.: Cloud condensation nuclei production from nucleation events at a highly polluted region, Geophys. Res. Lett., 32, L06812, doi:10.1029/2004GL022092, 2005.

Laaksonen, A., Kulmala, M., O'Dowd, C. D., Joutsensaari, J., Vaattovaara, P., Mikkonen, S., Lehtinen, K. E. J., Sogacheva, L., Dal Maso, M., Aalto, P., Petäjä, T., Sogachev, A., Yoon, Y. J., Lihavainen, H., Nilsson, D., Facchini, M. C., Cavalli, F., Fuzzi, S., Hoffmann, T., Arnold, F., Hanke, M., Sellegri, K., Umann, B., Junkermann, W., Coe, H., Allan, J. D., Alfarra, M. R., Worsnop, D. R., Riekkola, M.-L., Hyötyläinen, T., and Viisanen, Y.: The role of VOC oxidation products in continental new particle formation, Atmos. Chem. Phys., 8, 2657–2665, doi:10.5194/acp-8-2657-2008, 2008.

Lambe, A. T., Zhang, J. Y., Sage, A. M., and Donahue, N. M., Controlled OH radical production via ozone-alkene reactions for use in aerosol aging studies, Environ. Sci. Technol., 41(7), 2357–2363, 2007.

Lide, D. R. (Ed.): CRC Handbook of Chemistry and Physics, 77th Edn., CRC Press, Boco Raton, FL, 1996.

Martin, S.: Phase transitions of aqueous atmospheric particles, Chem. Rev., 100, 3403–3453, 2000.

Mikhailov, E., Vlasenko, S., Martin, S. T., Koop, T., and Pöschl, U.: Amorphous and crystalline aerosol particles interacting with water vapor: conceptual framework and experimental evidence for restructuring, phase transitions and kinetic limitations, Atmos. Chem. Phys., 9, 9491–9522, doi:10.5194/acp-9-9491-2009, 2009.

Murray, B. J.: Inhibition of ice crystallisation in highly viscous aqueous organic acid droplets, Atmos. Chem. Phys., 8, 5423–5433, doi:10.5194/acp-8-5423-2008, 2008.

Odum, J. R., Hoffmann, T., Bowman, F., Collins, D., Flagan, R. C., and Seinfeld, J. H.: Gas/particle partitioning and secondary organic aerosol yields, Environ. Sci. Technol., 30, 2580–2585, 1996.

Pankow, J. F.: An absorption model of the gas/aerosol partitioning involved in the formation of secondary organic aerosol, Atmos. Environ., 28, 189–193, 1994.

Ristimäki, J., Virtanen, A., Rostedt, A., and Keskinen, J.: On-line measurement of size distribution and effective density of submicron aerosol particles, J. Aerosol Sci., 33, 1541–1557,

Title Page

Abstract | Introduction

Conclusions | References

Tables | Figures

|◄ | ►|

◄ | ►

Back | Close

Full Screen / Esc

Printer-friendly Version

Interactive Discussion

2002.

Rogers, L. N. and Reed, J.: The adhesion of particles indergoing elastic-plastic impact with a surface, J. Phys D: Appl. Phys., 17, 677–689, 1984.

Spracklen, D. V., Carslaw, K. S., Kulmala, M., Kerminen, V.-M., Mann, G. W., and Sihto, S.-L.: The contribution of boundary layer nucleation events to total particle concentrations on regional and global scales, Atmos. Chem. Phys., 6, 5631–5648, doi:10.5194/acp-6-5631-2006, 2006.

Stein, S. W., Turpin, J. B., Cai, X., Huang, P. F., and McMurry, P. H.: Measurements of relative humidity dependent bounce and density for atmospheric particles using DMA-impactor technique, Atmos. Environ., 28, 1739–1746, 1994.

Tunved, P., Hansson, H.-C., Kerminen, V.-M., Ström, J., Dal Maso, M., Lihavainen, H., Viisanen, Y., Aalto, P. P., Komppula, M., and Kulmala, M.: Science, 312, 261–263, 2006.

Virtanen, A., Joutsensaari, J., Koop, T., Kannosto, J., Yli-Pirilä, P., Leskinen, J., Mäkelä, J. M., Holopainen, J. K., Pöschl, U., Kulmala, M., Worsnop, D. R., and Laaksonen, A.: An amorphous solid state of biogenic secondary organic aerosol particles, Nature, 467, 824–827, 2010.

Vuorinen, T., Nerg, A. M., Ibrahim, M. A., Reddy, G. V. P., and Holopainen, J. K.: Emission of *Plutella xylostella*-induced compounds from cabbages grown at elevated CO_2 and orientation behavior of the natural enemies, Plant Physiol., 135, 1984–1992, 2004.

Yli-Ojanperä, J., Kannosto, J., Marjamäki, M., Keskinen, J.: Improving the nanoparticle resolution of the ELPI, Aerosol Air Qual. Res., 10, 360–366, 2010.

Zobrist, B., Marcolli, C., Pedernera, D. A., and Koop, T.: Do atmospheric aerosols form glasses?, Atmos. Chem. Phys., 8, 5221–5244, doi:10.5194/acp-8-5221-2008, 2008.

Title Page

Abstract | Introduction

Conclusions | References

Tables | Figures

◀◀ | ▶▶

◀ | ▶

Back | Close

Full Screen / Esc

Printer-friendly Version

Interactive Discussion

Table 1. Summary of plant chamber experiments. Values are determined at the beginning of trials (density during experiments ± standard deviation).

#	Experiment	VOC (ppb)	O_3 (ppb)	SO_2 (ppb)	TME (ppb)	RH (%)	T (°C)	Density $g\,cm^{-3}$
1	Pine + O_3	16.8	35	–	–	34	22	1.00 ± 0.06
2	Pine + OH + SO_2	107.6	35	22	35.2	31	22	1.10 ± 0.07

Full Screen / Esc

Printer-friendly Version

Interactive Discussion
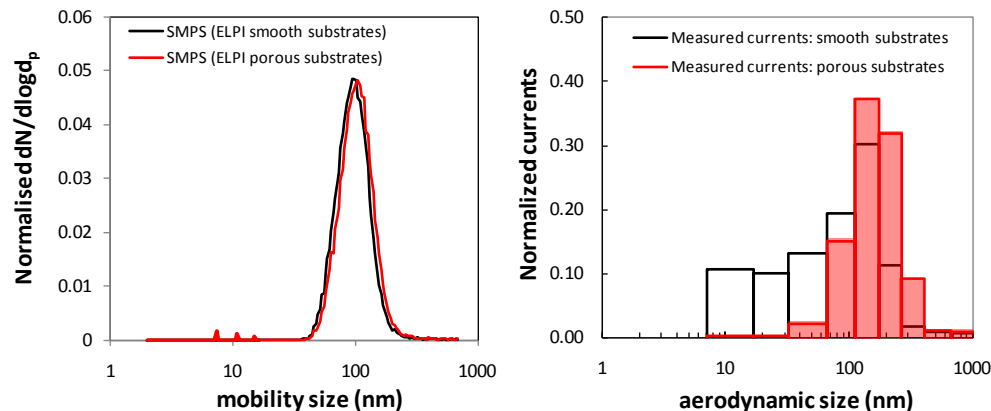
Fig. 1. (a) SMPS size distributions measured simultaneously with ELPI current distributions. **(b)** The ELPI current distributions measured by smooth (black-lined bars) and porous substrates (red bars) are shown as a function of particle diameter.
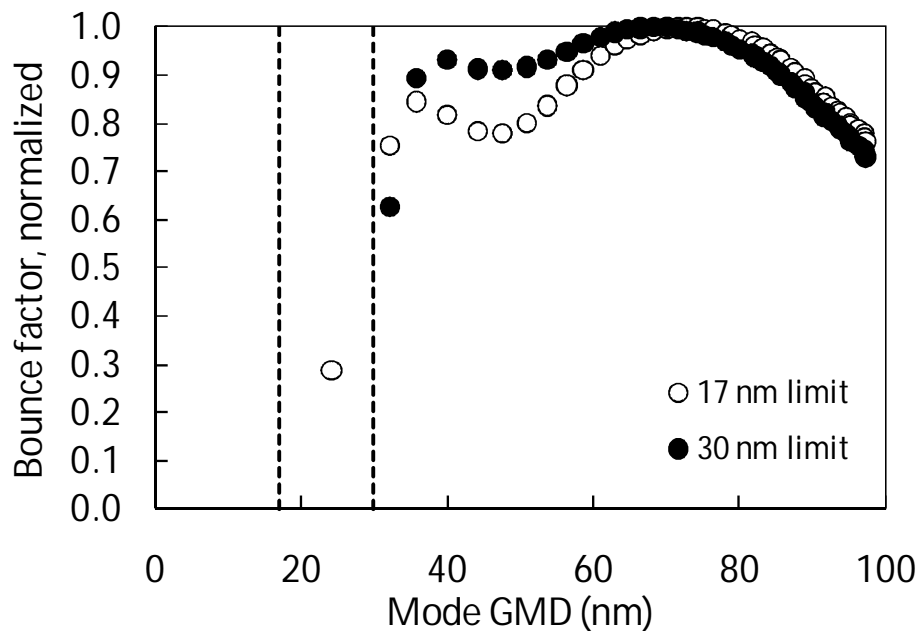
Fig. 2. Comparison of normalized bounce factors for measurements having 17 nm (open circles) and 30 nm (black dots) size limitations.
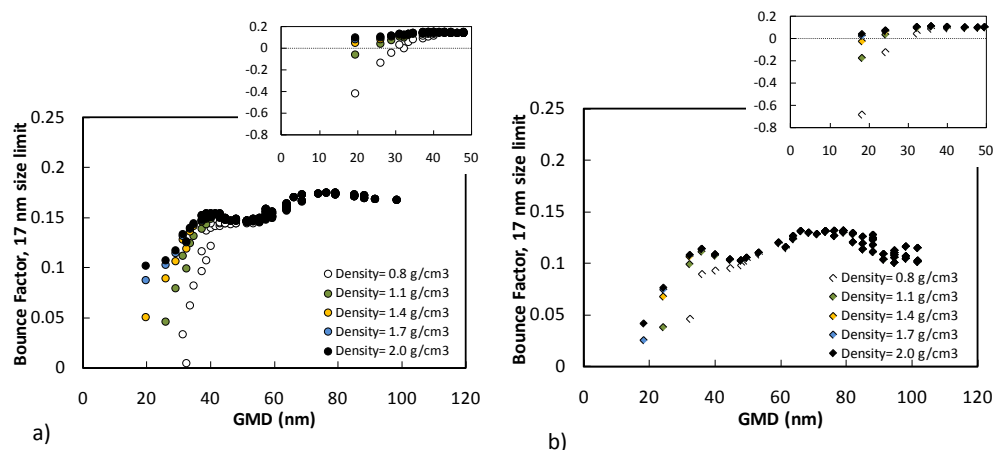
Fig. 3. Calculated bounce factors for the 17 nm size limit measured for **(a)** O_3 initiated oxidation in absence of SO_2 and **(b)** OH dominated oxidation in presence of SO_2. Density values varying from $0.8 \, \mathrm{g \, cm^{-3}}$ to $2 \, \mathrm{g \, cm^{-3}}$ were used in calculations. Insets in the upper right corners of **(a)** and **(b)** show details in bounce factor values for the smallest particles.
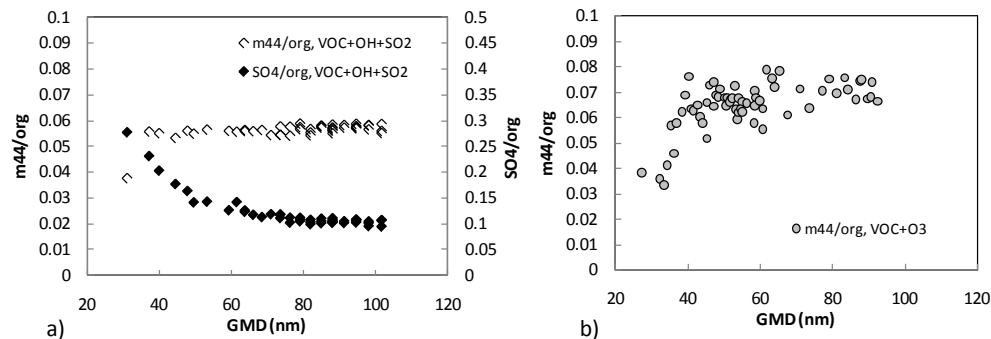
Fig. 4. m44/total organics ratio of particles derived from **(a)** OH initiated oxidation of the pine emitted VOCs, in the presence of SO_2, and **(b)** ozonolysis of the pine-emitted VOCs.